Sensors and Actuators B 160 (2011) 899–909

Contents lists available at SciVerse ScienceDirect

Sensors and Actuators B: Chemical

journal homepage: www.elsevier.com/locate/snb

On-line sensor calibration transfer among electronic nose instruments for monitoring volatile organic chemicals in indoor air quality

Lei Zhang, Fengchun Tian*, Chaibou Kadri, Bo Xiao, Hongjuan Li, Lina Pan, Hongwei Zhou

College of Communication Engineering, Chongqing University, 174 ShaPingBa District, Chongqing 400044, China

ARTICLE INFO

Article history:
Received 17 May 2011
Received in revised form 28 August 2011
Accepted 30 August 2011
Available online 8 September 2011

Keywords:
Electronic nose
Calibration transfer
Affine transformation
Kennard–Stone sequential algorithm
Robust weighted least square

ABSTRACT

Since the homogeneous linearity between multi-sensors systems which are called electronic noses (E-noses) designed using commercially available heated tin oxide sensors, a high performance of on-line calibration transfer among multiple E-nose instruments based on global affine transformation (GAT) and Kennard–Stone sequential algorithm (KSS) is presented and evaluated in this paper. GAT is achieved in terms of one single sensor by a robust weighted least square (RWLS) algorithm and KSS is studied for representative transfer sample subset selection from a large sample space. This paper consists of two aspects: calibration step (for responses of sensors) and prediction step (for gas concentration). Prediction is developed to evaluate the performance of calibration transfer. In prediction step, three artificial neural networks for concentration prediction of three analytes were trained based on an error back-propagation algorithm. Both implementations of the two aspects were operated on Matlab, preliminarily evaluated using hazardous formaldehyde as referenced gas and subsequently directly applied to quantify benzene and toluene which are measured by six E-nose instruments at specific gas experimental platform. Simulated and experimental results were found to be adequate and good precision and accuracy were obtained.

1. Introduction

Electronic nose (E-nose), which plays a major role in identification and quantification of the hazardous odors, has become a powerful tool to evaluate the odors during quality control process of foods and beverages [1–3], environment protection [4] and disease diagnostics [5]. E-nose is composed of gas sensors made from various materials that display distinct gas-sensing behaviors in which differentiation can be combined, and interpreted via pattern recognition techniques [6,7]. The sensors are mounted on a custom designed printed circuit board (PCB), along with associate electrical components. Among the available sensing materials, metal oxide semiconductor sensors [8] are perhaps the most ubiquitous gas sensors since they are used in most single gas monitors and in residential carbon monoxide detectors. However, a fundamental assumption is that the inherent variability during the sensor manufacturing process leads to slight differences in the reactivity of the tin oxide substrate of individual sensor [9]. For instance, when two identical sensors are exposed to the same environment, slightly different responses would be produced. One reason is that state-of-the-art gas-sensors do not maintain their sensitivity profile over time. Even brand new gas sensors, coming from the same production batch, may not generate identical response values when measuring identical samples. Other possible reasons are related to the physical environment (e.g. temperature, humidity and pressure). The whole purpose and why we do calibration in our work would be fully explained in the follows. As we know, traditional E-nose instruments which have a big volume are inconvenient and expensive to the users. Our project is devoted to design of portable E-nose used indoor so that many instruments should be produced for extensive users. However, in mass production of E-nose products such as air quality monitors, it is impossible to train an individual prediction model (e.g. ANN) on each E-nose product (instrument). However, it's convenient for us to construct an effective model on one standard instrument only (e.g. master) through a large amount of analytical chemical experiments. Unfortunately, due to the baseline differences of identical sensors, the developed prediction model using the chemical datasets on the master E-nose instrument may not be fitted with the datasets on other slave instruments even with completely the same sensor array and electrical components as the master instrument. Thereby, in real-time monitoring of environmental chemicals indoor, the displayed concentrations would not be identical and even false discriminations of gas concentrations for multiple instruments become possible. So, a well developed ANN with high prediction accuracy would lose adaptability with new instruments. Considering the intensive

* Corresponding author. Tel.: +86 23 65111745; fax: +86 23 65111745.
E-mail address: FengchunTian@cqu.edu.cn (F. Tian).

0925-4005/$ – see front matter © 2011 Elsevier B.V. All rights reserved.
doi:10.1016/j.snb.2011.08.079

complexity of repeated ANN train process for each instrument, it is impractical to construct one individual ANN for each instrument, respectively. Sensor calibration is therefore the first step during the mass developments of E-nose instruments. A good promotion of E-nose instruments for air quality monitoring should be based on a high performance of calibration transfer. Thus, on-line calibration transfer among E-nose instruments in mass production, with subsequent prediction of concentrations in unknown samples using electronic nose instruments has become increasingly important for manufacturers and researchers in Artificial Olfactory field. Manufacturers aim to construct instruments that generate exactly the same gas concentrations when exposed to identical environments. Until now, so many literatures on spectrophotometers instrument standardization based on transferring near-infrared (NIR) have been published, such as classical direct standardization (DS) and piece direct standardization (PDS) [10,11], orthogonal signal correction (OSC) [12], wavelet [13] and principle component regression (PCR) [14]. But these methods can only be used in the multidimensional E-nose system directly for off-line instrument calibration, because they should be implemented based on a data set, and also the robustness can also be promised when the responses of the sensors measured on a single instrument change over a period of time because of temperature and humidity fluctuation. That is to say, when the model studied based on a known data set is used to another new data set, the model would lose its effect. So, these methods cannot be used for on line calibration. However, so few literatures [15–17] on calibration transfer between electronic nose instruments with multidimensional sensor array in artificial olfactory fields inspire us to have a deep research on this issue toward attempting to solve the E-nose instrument related signal shift for on-line calibration. In the existent literatures, neural methods were used for sensor array calibration. Due to that a generalized neural network model should be based on a large number of transfer samples or datasets, it would certainly increase the experimental calibration complexity, especially in mass production. In this case, the neural methods would also become worthless. The on-line mass standardization is now still a bottleneck problem because of the multidimensional nonlinear characteristic of E-nose system.

The goal of this project is to develop a tin oxide sensor device (E-nose) capable of detecting and quantifying volatile organic chemicals present at typical indoor environments. In the previous publications [18–20], the E-nose sensor array and circuit device, feature selection and probabilistic neural network for wound classification have been researched through theoretical and experimental analysis. With knowledge of the approximated relation of linearity (homogeneous linearity) between two E-nose instruments with the same types of sensors, and the inherent flaws of the previous methods discussed above, a brand new method for on-line mass E-nose instruments calibration is proposed to realize the high-accuracy standardization between instruments in this paper. The applied methodology for calibration is global affine transformation (GAT) and Kennard–Stone sequential samples selection algorithm (KSS). Therein, the solutions of affine transformation coefficients is studied using a robust weighted least square (RWLS) algorithm and the sample selection is on the basis of Euclidean distance. Affine transformation was widely used for pattern matching [21,22]. The concentration prediction step is also developed for validation of the calibration transfer. Consider the strong nonlinearity of multi-sensors system internal (e.g. response and concentration), a feed forward multilayer perceptron neural network based on a back-propagation algorithm [23] is used for organic gas concentration prediction. As we know, artificial neural networks have been widely used for concentration prediction with electronic noses [24–26]. The main advantage of artificial neural network is that the heavy process of computation reduces significantly during the training [27]. It is worth mentioning that the back-propagation algorithm is a gradient-descent algorithm in which the network weights are moved along the negative direction of the performance function's gradient [28].

2. Theory

2.1. Calibration step

2.1.1. Affine transform based on RWLS

Affine transformation is a map F: $\Re^n \to \Re^n$ of the form $F(x) = \boldsymbol{A}^{\mathrm{T}}\boldsymbol{x} + \boldsymbol{t}$, for all $x \in \Re^n$, where $\boldsymbol{A}$ is a linear transformation of $\Re^n$ [29], and 'T' denotes transpose of matrix. Scaling, translation and rotation are included in affine transformation, but the first two (scaling and translation) are used here. Let $\boldsymbol{x}$ denote the dataset measured on the slaved E-nose instrument, and $\boldsymbol{y}$ the calibrated dataset from $\boldsymbol{x}$ to the master E-nose instrument. The calibration transfer model is shown as follow

$$\boldsymbol{y}_{i,n} = \boldsymbol{a}_i \cdot \boldsymbol{x}_{i,n} + \boldsymbol{b}_i, \quad i = 1, \ldots, k, \quad n = 1, \ldots, N \tag{1}$$

in which index i indicates the ith sensor, k denotes the number of sensors in the sensor array, index n represent the nth sample, N refers to the number of being calibrated samples; parameter $\boldsymbol{a}_i$ and $\boldsymbol{b}_i$ represent the on-line calibration transfer coefficients slope and intercept of the ith sensor, respectively. The coefficients are studied using hybrid robust weighted least square algorithm and KSS algorithm.

Robust weighted least square (RWLS) in this work is first applied to electronic nose datasets for accurately mapping one instrument (called "slave") to another (called "master") to realize instruments standardization. Assume the number of transfer samples is V, with knowledge of that ordinary least square (OLS) which is based on the minimum of square sum of error (SSE) is sensitive to outliers and therefore results in a failure in fuzzy chemical dataset measured using the nonlinear multivariate system. Interestingly, RWLS, which aims to reduce the sensitivity of SSE, can avoid the disadvantages of OLS through minimizing a weighted square sum of error (WSSE) [30] shown by

$$\min \sum_{v=1}^{V} w_v (y_v - \hat{y}_v)^2 \tag{2}$$

The re-weighted function "bi-square" is used in this work shown as follow

$$w_v = \begin{cases} (1 - u_v^2)^2, |u_v| < 1 \\ 0, |u_v| \geq \end{cases}, \quad v = 1, \ldots, V \tag{3}$$

where u_v is the adjusted residuals with standardization. This method minimizes a weighted sum of squares, in which the weight assigned to each sample point depends on how far the point is from the fitted line. The detailed procedure of *iterative RWLS algorithm* is presented as follows

Step 1: Fit the model using ordinary least square (OLS), and compute the initial error residual $\boldsymbol{r}_{\mathbf{1}\times\boldsymbol{V}}$.

Step 2: Compute the adjusted residuals using $r_{adj} = r_v/\sqrt{1 - h_v}$, $v = 1, \ldots, V$, where $\boldsymbol{r}$ is from *step* 1, $\boldsymbol{h}$ are leverages that adjust the residuals by down-weighting high leverage sample points that have a large effect on the least square fit. The leverages are the elements situated on the diagonal of the prediction matrix (hat matrix), defined as $\mathbf{H} = \boldsymbol{x}(\boldsymbol{x}^{\mathrm{T}}\boldsymbol{x})^{-1}\boldsymbol{x}^{\mathrm{T}}$; thus, the leverage $h_v = x_v(\boldsymbol{x}^{\mathrm{T}}\boldsymbol{x})^{-1}x_v{}^{\mathrm{T}}$, where x_v denotes the vth transfer sample point.

Step 3: Standardize the adjusted residuals from *step* 2 using $\boldsymbol{u} = \boldsymbol{r}_{adj}/K{\cdot}s$, where K is a tuning constant commonly set to 4.685,

and s is the robust variance given by MAD/0.6745, and MAD is the median absolute deviation of the residuals.
Step 4: Compute the updated robust weights in terms of the bi-square function of $\boldsymbol{u}$ described in Eq. (3).
Step 5: If the fit converges, algorithm terminated; otherwise, return to the *step* 1 for next iteration.

2.1.2. KSS algorithm for sample subset selection

In calibration, the selection of most representative samples that can reflect the whole sample space become necessary for building the model of Eq. (1). Therefore, the Kennard–Stone sequential algorithm [31] for sample selection is used in this work. Let $\boldsymbol{z}$ denote the dataset measured on the master instrument. In order to assure a uniform distribution of such a sample subset along the sensor response dataset space, KSS follows a stepwise procedure that new selections are taken in regions of the space far from the samples already selected in terms of the multivariate Euclidean distances $d_{\boldsymbol{z}}(p,q)$ between the response $\boldsymbol{z}$-vectors of each pair (p,q) of samples calculated as

$$d_z(p,q) = \sqrt{\sum_{i=1}^{k}[x_p(i) - x_q(i)]^2} \quad p,q \in [1,N] \tag{4}$$

The selection starts by taking the pair (p_1, p_2) of samples for which the distance $d_{\boldsymbol{z}}(p_1,p_2)$ is the largest. For clear understanding of this algorithm, the flow of *KSS algorithm* is described as follows:

Step 1: Set the desired number of transfer samples.
Step 2: Select the two furthest samples from each other in the whole sample space.
Step 3: Calculate the distances between other remaining samples and the selected ones; the nearest one for each pair is retained from all the pairs of distances.
Step 4: The sample with the furthest distance from these nearest distances retained in *step 2* is selected.
Step 5: Repeat *steps* 3 and 4 until the required number of transfer samples is achieved.

2.1.3. Application of the calibration model

The measurement data sets were divided into transfer set ($\mathbf{X_{tran}}$ for one slave instrument and $\mathbf{Z_{tran}}$ for the master instrument) and validation set ($\mathbf{X_{val}}$ for slave instrument and $\mathbf{Z_{val}}$ for master instrument). In calibration, $\mathbf{X_{tran}}$ and $\mathbf{Z_{tran}}$ with m transfer samples are used to design the standardization models ($m = 5$). The remaining p samples excluding that m transfer samples are used to validate the models ($p = 120$, in this paper). The transfer sets that contain m samples with k sensors ($k = 6$) are shown as follows

$$\mathbf{X_{tran}} = \begin{pmatrix} x_{11} & \cdots & x_{1k} \\ \vdots & \ddots & \vdots \\ x_{m1} & \cdots & x_{mk} \end{pmatrix}_{m\times k} \tag{5}$$

and

$$\mathbf{Z_{tran}} = \begin{pmatrix} z_{11} & \cdots & z_{1k} \\ \vdots & \ddots & \vdots \\ z_{m1} & \cdots & z_{mk} \end{pmatrix}_{m\times k} \tag{6}$$

The validation sets that contain p samples with k sensors are shown as follows

$$\mathbf{X_{val}} = \begin{pmatrix} x_{11} & \cdots & x_{1k} \\ \vdots & \ddots & \vdots \\ x_{p1} & \cdots & x_{pk} \end{pmatrix}_{p\times k} \tag{7}$$

and

$$\mathbf{Z_{val}} = \begin{pmatrix} z_{11} & \cdots & z_{1k} \\ \vdots & \ddots & \vdots \\ z_{p1} & \cdots & z_{pk} \end{pmatrix}_{p\times k} \tag{8}$$

After calibration on $\mathbf{X_{val}}$ of the slave instrument, the new corrected response matrix is indicated as

$$\mathbf{X_{val}} \overset{\text{after corrected}}{\longrightarrow} \mathbf{Y_{val}} = \begin{pmatrix} y_{11} & \cdots & y_{1k} \\ \vdots & \ddots & \vdots \\ y_{p1} & \cdots & y_{pk} \end{pmatrix}_{p\times k} \tag{9}$$

The mean relative difference (MRD) of the ith sensor shown below between the sensor response of the slaves ($\boldsymbol{x}$, before calibration; $\boldsymbol{y}$, after calibration) and the sensor response $\boldsymbol{z}$ of the master instrument is performed as the evaluation measure of the proposed calibration model.

$$MRD_i = \frac{1}{N}\sum_{n=1}^{N}\left|\frac{x_{i,n} - z_{i,n}}{z_{i,n}}\right| \propto \frac{1}{N}\sum_{n=1}^{N}\left|\frac{y_{i,n} - z_{i,n}}{z_{i,n}}\right| \tag{10}$$

For the purpose of clarity, as we know, when the calibration model is used to other new systems, some prior information of each new system should be known. So, five transfer samples should be obtained through experiments using that new instrument being calibrated. Then, the proposed calibration model can be used to determine the calibrated coefficients of the new instrument.

2.2. Prediction step

Multilayer perceptron feed forward neural network based on error back-propagation algorithm is applied for organic chemicals concentration prediction in our project. The prediction benefits from the strong generalization ability for approximation of artificial neural network and its low computation complexity for a large number of multidimensional experimental datasets. For predicting concentration, we adopt the multi-input and single-output neural network to solve the approximation between responses of the sensors and concentrations of the odor. Three layered neural network m-h-o (one input layer with m neurons, one hidden layer with h neurons and one output layer with o neurons) is used in experience. The neural network can be illustrated through weight matrix $\mathbf{W_1}(m \times h)$, $\mathbf{W_2}(h \times o)$, and bias vector $\mathbf{B_1}(h \times 1)$, $\mathbf{B_2}(o \times 1)$ ($o = 1$, in this paper). The architecture of the neural network is illustrated in Fig. 1.

Given the responses $\boldsymbol{z}$ (training samples measured on the master instrument) and the training targets $\mathbf{T}$ (actual concentrations of analytes), the train process of ANN is employed for the weight matrix and bias vectors learning. The training weights $\mathbf{W_1}$, $\mathbf{B_1}$, $\mathbf{W_2}$ and $\mathbf{B_2}$ are first achieved through the back-propagation algorithm. Detailed description of neural networks is out of the scope of this present study; for that, we refer the reader to [23,27] for clearly understand the training procedure or learning process through back-propagation algorithm. The active functions of the hidden layer and output layer for that approximation are selected as log-sigmoid and pure linear function. After training, the forward computation process for predicted concentration is shown as follows.

The output of the jth hidden node is calculated by the log-sigmoid transfer function

$$f(node_j) = \frac{1}{1 + e^{-\left(\sum_{i=1}^{m} w_{ij}\cdot z_i - b_j\right)}} \quad j = 1,\ldots,h \tag{11}$$

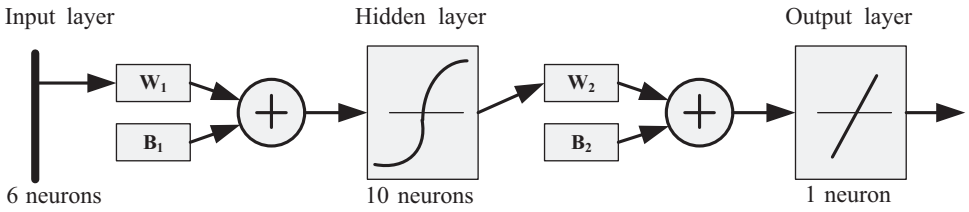

Fig. 1. Type of architecture of the neural network.

where w_{ij} (one element of $\mathbf{W_1}$) is the connection weight from the ith node of input layer to the jth node of hidden layer, and b_j (one element of $\mathbf{B_1}$) is the bias of the jth hidden layer.

The output concentration of the kth output node is calculated by the pure linear function

$$\varphi_k = \sum_{j=1}^{h} w_{kj} \cdot f(node_j) - b_k, \quad k = 1, \ldots, o \tag{12}$$

where w_{kj} (one element of $\mathbf{W_2}$) is the connection weight from the jth hidden node to the kth output node, b_k (one element of $\mathbf{B_2}$) is the bias of the kth output layer.

The learning error E can be calculated by the following formulation

$$E = \sum_{c=1}^{q} \frac{E_c}{(q \cdot o)} \quad \text{where} \quad E_c = \sum_{k=1}^{o} (y_k^c - T_k^c)^2, \tag{13}$$

where q is the number of total training samples, $y_k^c - T_k^c$ is the error of the actual output and desired output of the kth output unit when the cth training sample is used for training.

In performance evaluation, root mean square error of prediction (*RMSEP*) and mean absolute relative error of prediction (*MAREP*) (similar to Ref. [31,32]) are used to verify the calibration effect through concentration prediction. The *RMSEP* is calculated as

$$RMSEP = \sqrt{\frac{1}{N} \sum_{n=1}^{N} (\varphi_n - T_n)^2} \tag{14}$$

The *MAREP* is calculated as

$$MAREP = \frac{1}{N} \sum_{n=1}^{N} \left| \frac{\varphi_n - T_n}{T_n} \right| \tag{15}$$

where φ_n and T_n denote the predicted and actual concentration for the nth sample, respectively.

3. Experimental

3.1. Electronic nose module

The metal oxide semiconductor gas sensors used in our e-nose system consist of TGS series from FIGARO, USA. They are TGS2602, TGS2620 and TGS2201 with two outputs A and B (TGS2201A/B). In addition, a module (SHT2230 of Sensirion in Switzerland) with two auxiliary sensors for temperature and humidity compensations is also used. The sensors were mounted on a custom designed printed circuit board (PCB), along with associated electrical components. An analog-digital converter (AD) is used as interface between the FPGA processor and the sensors. The system can be connected to a PC via a JTAG port. An additional flash memory is used to save the weights and biases of the neural network trained on the PC and the calibration transfer coefficients of each sensor. The data sets for these gases are made up of samples in $\Re^6$ space, it just means that an input vector with 6 independent variables was obtained in each observation. The gases measurements are implemented in the Constant Temperature and Humidity chamber (LRH-150S) in which the temperature and humidity can be effectively controlled in terms of the desired temperatures and humidity. In this paper, six E-nose instruments with completely identical types of sensors and electrical components are used for verifying the proposed calibration model. For convenience of subsequent analysis, one instrument is selected as the "master" which is recognized as the standard instrument and the left five are named as "slave_1, slave_2, slave_3, slave_4, slave_5" which will be calibrated according to [10]. It is worth noting that all the six instruments would employ the experiments together at the same time in the chamber to ensure the consistence of the experimental samples on each instrument.

3.2. Gas datasets

Three organic chemicals have been analyzed in calibration step and prediction step: formaldehyde, benzene and toluene. The experiments of sample collections are developed in the chamber. The E-nose instrument should be exposed to each of the three candidates in many different concentrations separately, and the responses of the sensors are saved on PC in each measurement. Totally, 243 measurements (dataset) including 125 formaldehyde samples, 52 benzene samples and 66 toluene samples for each instrument are measured in the same way. These samples are measured through different combinations of the target temperatures of 15, 25, 30 and 35 °C and target humidity of 40, 60, 80 RH. The total measurement cycle time for a single measurement was set to 10 min, i.e. 2 min reference air (baseline) and 8 min sampling. Between two single measurements, 10 min for cleaning the chamber through injecting clean air are also consumed. In one single measurement, the temperature and humidity have little change except the slightly fluctuation. Note that the calibration and prediction variables (features) used in our work are the steady state responses. Fig. 2 illustrates the experimental response process of the gas sensors at a time and the locations of steady state response selected as features of the gas sensors have also been pointed out.

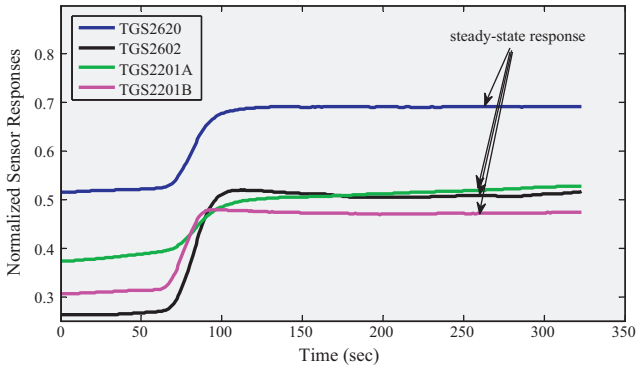

Fig. 2. Normalized sensor responses versus time with sensors exposed to hazardous air.

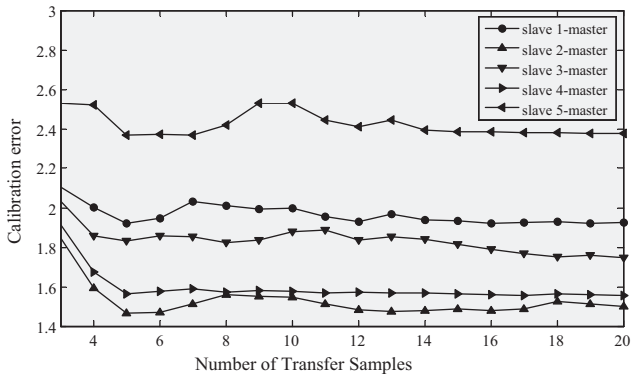

Fig. 3. Performance of calibration with increasing number of transfer samples.

In the studies of calibration models, formaldehyde was chosen as referenced gas.

4. Results and discussion

4.1. Sensor response calibration

Sensor response calibration indicates the projections from the response of slave instruments to the response of the master instrument. For on-line calibration among E-nose instruments, we select formaldehyde as reference gas and a certain number of transfer samples are also needed for developing the calibration coefficients using the hybrid RWLS and KSS algorithm. Fig. 3 studies the calibration error (MRD in Eq. (10) of all sensors between slave instruments and the master after calibration) when using different number of transfer samples. We can see that five transfer samples are enough to perform a good calibration. More transfer samples would also increase the experimental and calibration complexity in mass production. Fig. 4 illustrates the linear regression curves of each sensor between the slave_5 and the master using hybrid RWLS and KSS algorithm on the selected five transfer samples. Each sub-figure in Fig. 4 represents one type of sensor. Fig. 4 also demonstrates the homogeneous linearity between multi-sensors systems and feasibility of the proposed calibration transfer model.

Table 1 also presents the regression coefficients of another four slaves (from slave_1 to slave_4). All squared correlation coefficient r^2 values are between 0.967 and 0.998 and there was no statistically significant difference ($\alpha = 0.05$) between the master instrument responses and calibrated responses from the slave instruments. Its worth noting that all the instruments should use the same transfer sample number (*index* 1, . . ., 5) obtained from the master dataset by calling the KSS algorithm, namely, in subsequent calibration of other slaves (from slave_1 to slave_5), the same samples number (*index* 1, . . ., 5) should be used.

Table 2 presents the performance validation error of the remaining 120 formaldehyde samples using the calibration coefficients described in Fig. 4 and Table 1. Figs. 5–10 illustrate the steady state response curves (single sensor) of the 120 formaldehyde samples measured on the 6 instruments together, respectively; (a) denotes the 6 curves before calibration; (b) denotes the 6 curves after calibration. That line with circles is the steady state response curve of the master instrument which is recognized as the calibration targets. In Table 2, the columns labeled "N" denote the mean relative difference (MRD) of all sensors and samples between the slave instruments and the master without calibration, while the columns labeled "Y" is with calibration. Through Table 2 and these figures (Figs. 5–10), we can find that the calibration coefficients developed

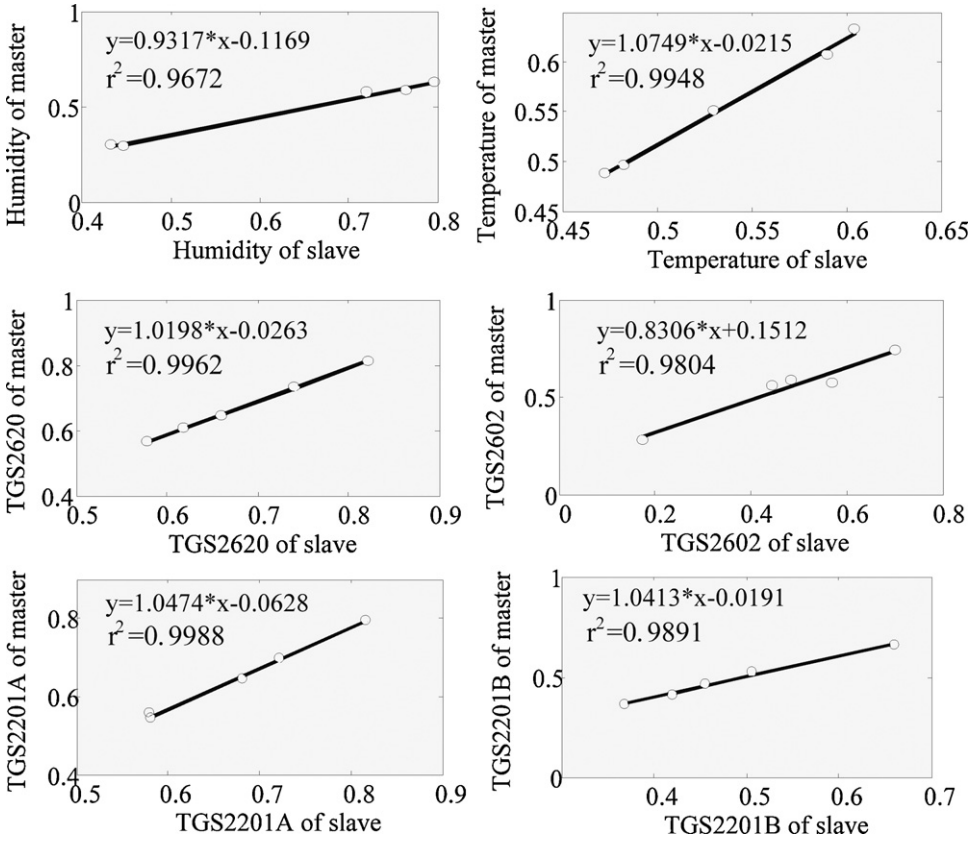

Fig. 4. Calibration regression equations between slave_5 and the master using RWLS estimator and five representative transfer samples selected by KSS algorithm. In each sub-figure, the open symbols are the selected five transfer sample points; the line is the regression of the five points.

Table 1
Calibration transfer regression coefficients (calibration equation, $y = ax + b$).

Sensor	slave_1-master			slave_2-master			slave_3-master			slave_4-master		
	a	b	r^2	a	b	r^2	a	b	r^2	a	b	r^2
Humidity	0.9280	0.0136	0.9736	1.0073	−0.1056	0.9600	0.9903	−0.0091	0.9798	0.8125	0.0472	0.9714
Temperature	0.9929	0.0032	0.9952	1.0510	−0.0213	0.9974	1.0714	−0.0399	0.9944	0.9799	0.0220	0.9963
TGS2620	1.0126	−0.0156	0.9975	0.9848	0.0157	0.9939	1.0069	−0.0071	0.9988	1.0009	−0.0097	0.9983
TGS2602	0.9291	0.0540	0.9753	0.9482	0.0409	0.9922	0.8326	0.1178	0.9725	0.9161	0.0924	0.9778
TGS2201A	1.0687	−0.0666	0.9885	1.0516	−0.0581	0.9835	1.1283	−0.1323	0.9812	0.9719	0.0032	0.9913
TGS2201B	1.0381	−0.0671	0.9876	1.0356	−0.0317	0.9958	1.0030	−0.0254	0.9931	1.0096	−0.0272	0.9880

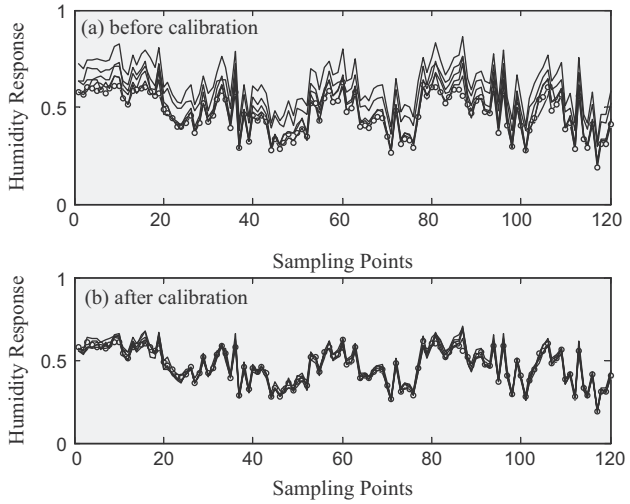

Fig. 5. Humidity sensor responses with 120 samples measured before and after calibration; six curves including five slaves and the master.

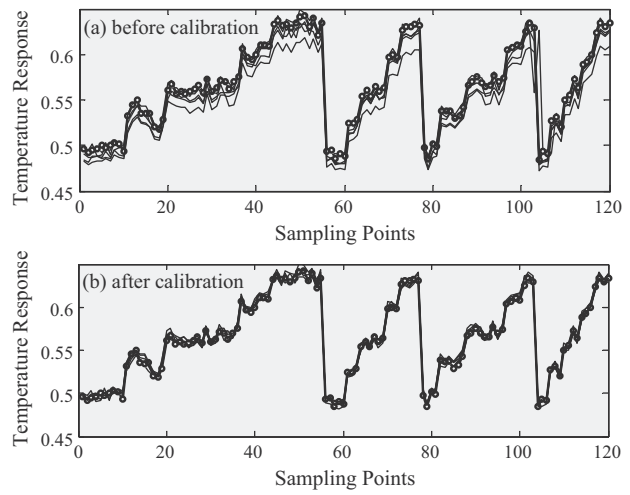

Fig. 6. Temperature sensor responses with 120 samples measured before and after calibration; six curves including five slaves and the master.

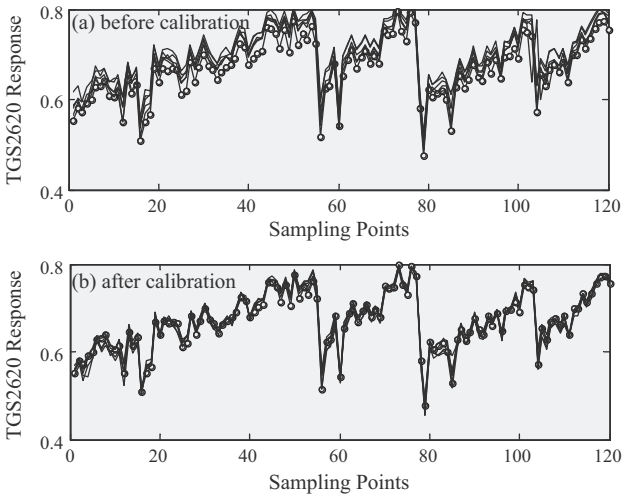

Fig. 7. TGS2620 responses with 120 samples measured before and after calibration; six curves including five slaves and the master.

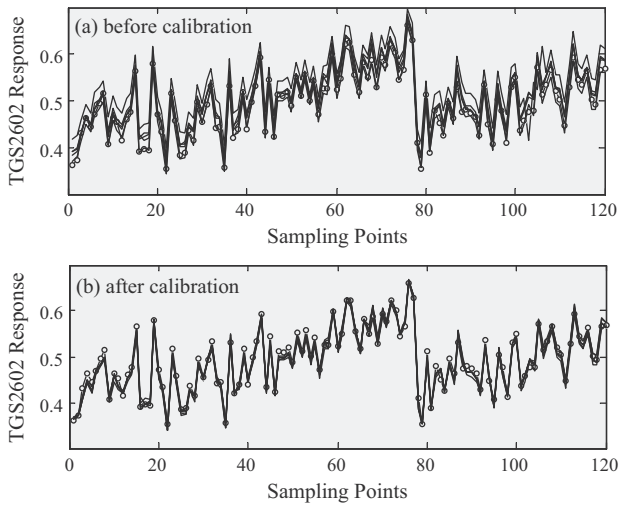

Fig. 8. TGS2602 responses with 120 samples measured before and after calibration; six curves including five slaves and the master.

Table 2
Mean relative difference (MRD) of each sensor between the master instrument and the slaves.

Sensor	Master-slave_1		Master-slave_2		Master-slave_3		Master-slave_4		Master-slave_5	
	N	Y	N	Y	N	Y	N	Y	N	Y
Humidity	0.0550	0.0354	0.0968	0.0301	0.3539	0.0333	0.0439	0.0266	0.3038	0.0866
Temperature	0.0054	0.0047	0.0171	0.0052	0.0325	0.0055	0.0088	0.0041	0.0628	0.0162
TGS2620	0.0113	0.0032	0.0149	0.0057	0.0183	0.0047	0.0042	0.0026	0.0063	0.0038
TGS2602	0.0468	0.0242	0.1003	0.0226	0.1202	0.0324	0.0826	0.0286	0.0248	0.0132
TGS2201A	0.0347	0.0224	0.0309	0.0111	0.0535	0.0117	0.0594	0.0155	0.0245	0.0113
TGS2201B	0.0981	0.0298	0.0384	0.0110	0.0221	0.0207	0.0368	0.0171	0.0284	0.0128

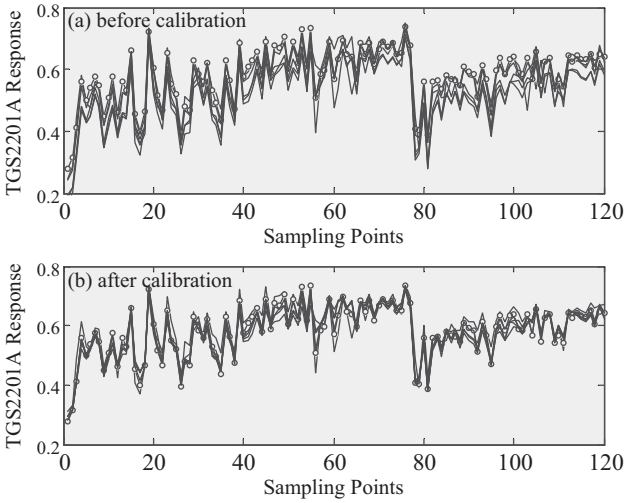

Fig. 9. TGS2201A responses with 120 samples measured before and after calibration; six curves including five slaves and the master.

using the selected five transfer samples successfully realized the on-line response projections.

The responses of the master instrument are denoted by the line with circles, and other five slaves aim to approximate the master instrument by the calibration transfer coefficients. In actual applications of these five slave instruments, the calibration coefficients $\boldsymbol{a}$, $\boldsymbol{b}$ would be saved on each slave instrument for on-line automated calibration. In mass production, all the slaves should be first located in specific experimental environment in accordance with the selected five transfer samples (*index* 1, . . ., 5) measured on the master instrument for determining the projection parameters of each slave instrument.

4.2. Concentration prediction

In this section, the concentration prediction model is constructed using the dataset measured on the master E-nose instrument using multilayered feed-forward artificial neural network trained by error back-propagation algorithm. The train process of ANN is automatically operated using Matlab toolbox of neural network. The concentration prediction is also studied mainly to find out the improved fitting ability of the five slaves when still using the same prediction model as the master after

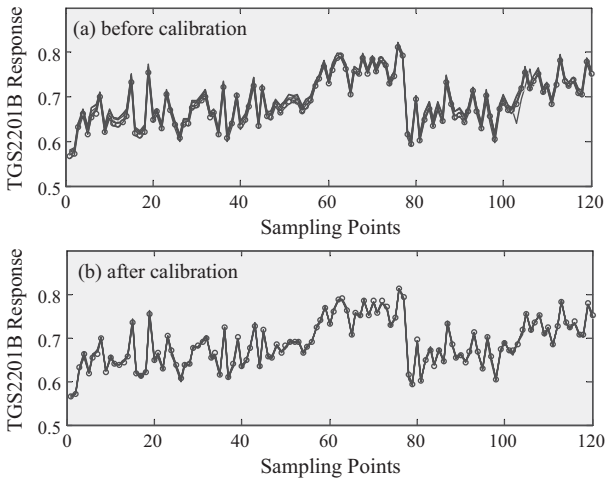

Fig. 10. TGS2201B responses with 120 samples measured before and after calibration; six curves including five slaves and the master.

using the presented on-line calibration transfer; in this case, the importance and necessity of calibration transfer have also been demonstrated. In this section, three organic chemicals datasets were used for concentration measure: formaldehyde, benzene and toluene. Thus, three single ANNs (ANN_1, ANN_2 and ANN_3) were built for these three analytes, and the three ANNs should be trained on their gas dataset individually. Considering the generalization of ANNs, three sets of samples for each analyte have been classified: training set, monitoring set and test set [28]. The monitoring set is used to control the training process and avoid overfitting. In this paper, the predicted and actual concentrations of 20 test samples for each analyte are presented to test our calibration model. The validation must be performed with the test set, composed of samples not used in the ANN train and monitor. Once trained, the obtained weights $\mathbf{W_1}$, $\mathbf{W_2}$ and bias vectors $\mathbf{B_1}$, $\mathbf{B_2}$ should be saved on each E-nose instrument for calculating the concentrations of analytes in real-time using Eqs. (11) and (12). The parameters of each ANN consist of 6 input neurons, 10 hidden neurons and 1 output neuron (see Fig. 1). The maximum number of epochs is set as 2000 and the convergence goal of each epoch in the training process is set randomly between 0.0005 and 0.05.

Tables 3–5 present the formaldehyde concentrations of 20 test samples including the five slave instruments, the master instrument and the actual (reference). To each table, the columns labeled "*N*" denote the predicted concentration without calibration process; while the columns labeled "*Y*" denote the predicted concentration with calibration. It is worthy noting that the predicted concentration values on each slave instrument are calculated using the same ANN_1, ANN_2 and ANN_3 as the master instrument. In visual, Figs. 11–13 illustrate the predicted concentration curves of 20 test samples (slave_1, 2, 3, 4 and 5, master and actual) of three analytes, respectively; (a) denotes the predicted and actual concentrations before calibration, and (b) denotes the same results as (a) after calibration.

The line with circles denotes the actual concentrations (reference); the line with triangles indicates the predicted concentrations of the master. Through Tables 3–5 and Figs. 11–13, we can find that the predicted concentrations of the five slaves after calibration become more close to the master and actual concentrations than before. Also, we can believe that the calibration transfer coefficients employed from slaves to the master can be fitted with formaldehyde, benzene and toluene. For error quantifications, Tables 6 and 7 present the RMSEP and MAREP values of the three measured analytes. Therein, the columns labeled "*N*" and "*Y*" denote the results without and with calibration, respectively.

From the above two tables (Tables 6 and 7), the RMSEP and MAREP of predicted concentrations on the three analytes are reduced significantly after calibration. The fitting ability of the slaves to the prediction model trained on the master instrument has been strengthened obviously. Thus, all the E-nose instruments for air quality monitoring can share the same prediction model (weights and biases of ANN) as the master instrument, and avoid the repeated and complex ANN train process on each instrument.

In mass production, the on-line sensor calibration method proposed here is based on a global affine transformation. The difference between global and local affine transformation is that the slave instruments are calibrated in the whole sample space without considering the piecewise linearity. Local transformation (e.g. piecewise) can also be used in terms of different conditions (e.g. types of hazardous gases and concentrations of gases). Through experimental analysis, we find that the calibration model constructed by formaldehyde can also be directly applied to benzene and toluene. For these three analytes, low, middle and high concentration predictions have been tested for calibration based on global affine transformation. Note that acquirement of representative transfer samples using KSS algorithm should be built in a

Table 3
Test of formaldehyde concentration estimation (concentration in ppm).

Sampling number	slave_1		slave_2		slave_3		slave_4		slave_5		Master	Actual
	N	*Y*	*N*	*Y*	*N*	*Y*	*N*	*Y*	*N*	*Y*	–	–
1	0.084	0.066	0.086	0.067	0.558	0.064	0.123	0.067	0.026	0.064	0.067	0.064
2	0.068	0.076	0.070	0.076	0.109	0.080	0.111	0.081	0.116	0.084	0.074	0.074
3	0.666	0.090	0.364	0.100	0.959	0.098	0.114	0.085	0.734	0.120	0.079	0.081
4	0.114	0.082	0.126	0.083	0.800	0.086	0.118	0.091	0.477	0.095	0.080	0.090
5	0.061	0.094	0.075	0.087	0.115	0.105	0.139	0.094	0.113	0.090	0.096	0.103
6	0.061	0.163	0.084	0.159	0.129	0.140	0.204	0.130	0.158	0.138	0.140	0.140
7	1.030	0.300	0.163	0.115	0.439	0.126	0.813	0.190	0.813	0.195	0.188	0.172
8	0.221	0.164	0.096	0.200	0.236	0.198	0.348	0.182	0.583	0.166	0.181	0.174
9	0.012	0.123	0.088	0.172	0.148	0.162	0.293	0.162	0.137	0.180	0.180	0.196
10	0.033	0.117	0.084	0.241	0.109	0.118	0.179	0.201	0.239	0.201	0.185	0.206
11	0.418	0.236	0.447	0.422	1.040	0.230	0.233	0.244	1.130	0.266	0.256	0.234
12	0.079	0.207	0.004	0.234	0.577	0.206	1.236	0.312	1.687	0.200	0.216	0.250
13	1.268	1.497	0.598	1.361	2.274	1.193	1.684	1.529	1.594	1.300	1.387	1.419
14	1.243	1.892	0.172	1.581	0.959	1.512	2.000	1.484	2.618	1.523	1.816	1.753
15	1.574	2.125	2.322	2.132	2.380	1.950	1.984	2.100	0.153	2.237	2.127	2.191
16	2.012	2.113	2.267	2.559	3.251	1.964	2.031	2.160	1.668	1.938	2.481	2.456
17	2.464	2.765	0.176	2.503	1.442	2.382	2.019	2.133	3.152	2.582	2.461	2.615
18	2.763	3.340	2.547	3.219	2.467	2.557	2.752	2.833	3.323	3.146	3.216	3.169
19	3.035	3.894	1.311	4.211	3.151	4.094	4.746	4.612	4.057	4.837	4.539	4.529
20	5.283	5.307	5.099	5.320	4.425	5.314	5.309	5.314	5.302	5.315	5.318	5.322

Table 4
Test performance of benzene concentration estimation (concentration in ppm).

Sampling number	slave_1		slave_2		slave_3		slave_4		slave_5		Master	Actual
	N	*Y*	*N*	*Y*	*N*	*Y*	*N*	*Y*	*N*	*Y*	–	–
1	0.126	0.181	0.131	0.180	0.207	0.184	0.127	0.179	0.236	0.170	0.181	0.172
2	0.172	0.278	0.232	0.283	0.451	0.275	0.276	0.324	0.302	0.281	0.301	0.281
3	0.342	0.499	0.400	0.522	0.680	0.529	0.416	0.513	0.534	0.517	0.519	0.500
4	0.696	0.861	0.810	0.910	1.259	0.873	0.770	0.860	0.884	0.833	0.918	0.911
5	0.114	0.179	0.054	0.179	0.023	0.222	0.014	0.235	0.105	0.168	0.165	0.172
6	0.189	0.287	0.246	0.300	0.367	0.303	0.224	0.310	0.264	0.294	0.279	0.281
7	0.335	0.442	0.483	0.507	0.712	0.454	0.435	0.487	0.418	0.493	0.499	0.500
8	0.725	0.871	0.974	0.922	1.288	0.840	0.787	0.872	1.002	0.922	0.956	0.911
9	0.125	0.220	0.157	0.182	0.323	0.196	0.217	0.195	0.245	0.216	0.199	0.172
10	0.303	0.492	0.361	0.524	0.698	0.512	0.427	0.510	0.562	0.502	0.490	0.500
11	0.668	0.893	0.776	0.916	1.010	0.876	0.618	0.900	0.797	0.891	0.897	0.911
12	0.108	0.181	0.156	0.179	0.327	0.181	0.199	0.185	0.250	0.191	0.183	0.172
13	0.149	0.301	0.242	0.277	0.414	0.294	0.253	0.305	0.272	0.303	0.301	0.281
14	0.352	0.463	0.401	0.505	0.745	0.512	0.455	0.511	0.511	0.470	0.538	0.500
15	0.715	0.928	0.804	0.932	0.909	0.845	0.556	0.900	0.784	0.876	0.873	0.911
16	0.098	0.170	0.147	0.183	0.253	0.211	0.155	0.188	0.317	0.236	0.209	0.172
17	0.146	0.272	0.215	0.294	0.377	0.256	0.231	0.266	0.265	0.259	0.272	0.281
18	0.233	0.469	0.343	0.467	0.592	0.445	0.362	0.512	0.370	0.363	0.429	0.500
19	0.683	0.845	0.802	0.923	1.080	0.868	0.661	0.801	0.748	0.763	0.912	0.911
20	0.065	0.174	0.077	0.176	0.264	0.172	0.161	0.172	0.133	0.168	0.149	0.172

Table 5
Test performance of toluene concentration estimation (concentration in ppm).

Sampling number	slave_1		slave_2		slave_3		slave_4		slave_5		Master	Actual
	N	*Y*	*N*	*Y*	*N*	*Y*	*N*	*Y*	*N*	*Y*	–	–
1	0.068	0.055	0.059	0.054	0.065	0.053	0.047	0.055	0.067	0.051	0.055	0.052
2	0.069	0.043	0.047	0.049	0.077	0.048	0.075	0.049	0.066	0.045	0.049	0.052
3	0.183	0.092	0.098	0.084	0.120	0.092	0.107	0.093	0.149	0.086	0.090	0.086
4	0.292	0.149	0.152	0.148	0.191	0.143	0.175	0.142	0.294	0.140	0.147	0.143
5	0.076	0.062	0.072	0.067	0.076	0.062	0.076	0.059	0.074	0.059	0.063	0.067
6	0.093	0.069	0.077	0.063	0.088	0.070	0.087	0.064	0.099	0.068	0.073	0.067
7	0.157	0.134	0.101	0.137	0.129	0.139	0.123	0.134	0.189	0.131	0.132	0.143
8	0.084	0.062	0.063	0.055	0.088	0.062	0.087	0.060	0.093	0.063	0.065	0.052
9	0.109	0.067	0.079	0.068	0.099	0.067	0.094	0.063	0.124	0.071	0.073	0.076
10	0.276	0.132	0.153	0.141	0.189	0.131	0.172	0.111	0.330	0.142	0.148	0.143
11	0.082	0.057	0.049	0.052	0.075	0.050	0.063	0.046	0.067	0.047	0.052	0.052
12	0.107	0.063	0.075	0.064	0.095	0.059	0.087	0.056	0.121	0.065	0.063	0.067
13	0.106	0.066	0.074	0.064	0.093	0.064	0.086	0.058	0.102	0.062	0.067	0.067
14	0.267	0.124	0.138	0.129	0.177	0.122	0.161	0.103	0.312	0.127	0.128	0.133
15	0.078	0.059	0.053	0.058	0.076	0.055	0.065	0.059	0.076	0.053	0.059	0.067
16	0.108	0.071	0.070	0.075	0.098	0.071	0.089	0.063	0.131	0.071	0.076	0.076
17	0.207	0.109	0.116	0.137	0.161	0.116	0.152	0.097	0.286	0.122	0.131	0.143
18	0.097	0.051	0.057	0.048	0.094	0.059	0.087	0.058	0.122	0.051	0.054	0.052
19	0.097	0.061	0.059	0.069	0.095	0.059	0.085	0.057	0.129	0.062	0.064	0.067
20	0.129	0.068	0.067	0.076	0.108	0.066	0.095	0.061	0.186	0.073	0.074	0.076

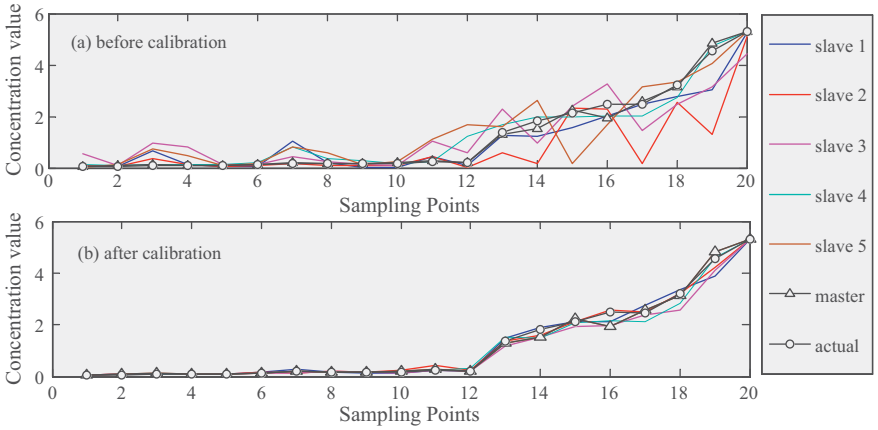

Fig. 11. Performance of predicted concentrations on test samples (before and after calibration) of formaldehyde.

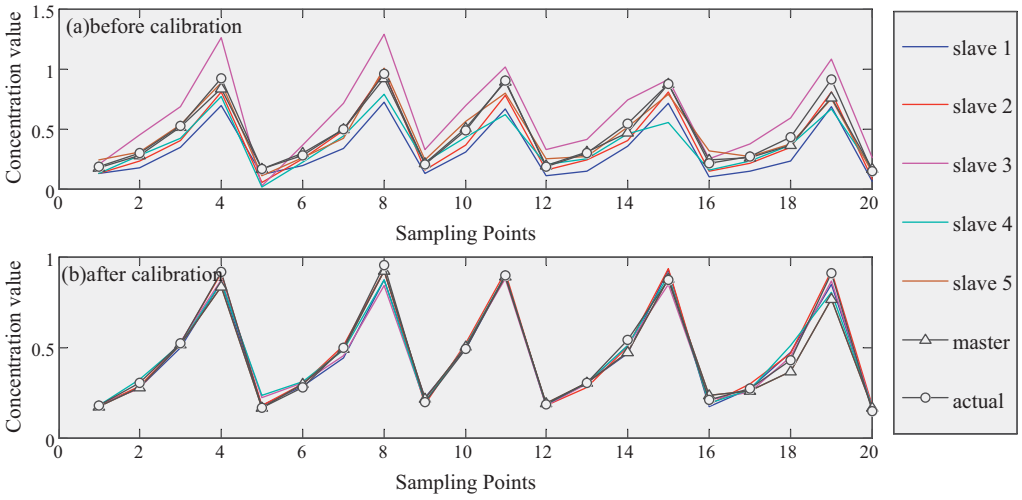

Fig. 12. Performance of predicted concentrations on test samples (before and after calibration) of benzene.

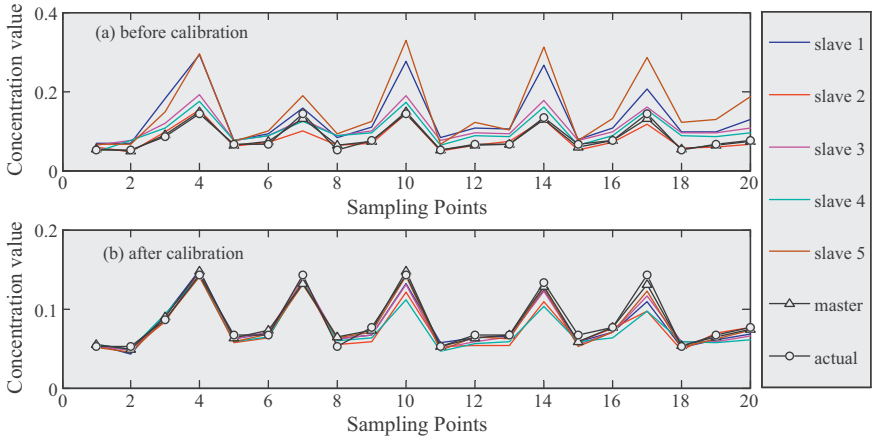

Fig. 13. Performance of predicted concentrations on test samples (before and after calibration) of toluene.

Table 6
RMSEP of the three measured analytes.

RMSEP	slave_1-actual		slave_2-actual		slave_3-actual		slave_4-actual		slave_5-actual		Master–actual
	N	*Y*	*N*	*Y*	*N*	*Y*	*N*	*Y*	*N*	*Y*	–
Formaldehyde	0.4743	0.1782	1.0048	0.1014	0.6695	0.2282	0.3440	0.1641	0.7113	0.1484	0.0439
Benzene	0.1580	0.0299	0.0880	0.0140	0.1782	0.0363	0.1386	0.0358	0.0828	0.0535	0.0269
Toluene	0.0655	0.0101	0.0136	0.0041	0.0294	0.0093	0.0214	0.0163	0.0866	0.0078	0.0059

Table 7
MAREP of the three measured analytes.

MAREP	slave_1-actual		slave_2-actual		slave_3-actual		slave_4-actual		slave_5-actual		Master–actual
	N	*Y*	*N*	*Y*	*N*	*Y*	*N*	*Y*	*N*	*Y*	–
Formaldehyde	18.744	2.8550	12.000	2.6549	37.100	2.5408	13.253	1.7031	32.094	1.9712	0.9720
Benzene	7.0101	1.0626	4.0642	0.6454	8.5268	1.5997	4.3465	1.4660	4.1445	1.7059	1.2842
Toluene	11.211	1.7730	2.4016	0.8488	7.0995	1.8126	5.1516	2.6932	14.517	1.4781	1.1507

big enough sample space so that the selected transfer samples can represent the whole range of concentrations being monitored. However, calibration accuracy may be reduced slightly. The experimental results demonstrate the good performance of global calibration transfer. Consider the unknown concentration of hazardous gas in real-time, its difficult for local affine transformation to determine different calibration model using piecewise linearity in terms of different stages of concentrations, and it needs a further research in the future work.

5. Conclusions

Due to the instrumental signal shift, when used the well studied concentration prediction network based on the referenced master instrument, the new instrument can not perform good concentration prediction or even display false concentrations. So, this paper addresses the critical issue of calibration transfer among electronic nose instruments based on the assumption that homogeneous linearity of E-nose multi-sensors system. A high performance of on-line sensor calibration transfer model used for indoor air quality monitoring through global affine transformation based on robust weighted least square algorithm and Kennard–Stone sequential sample subset selection algorithm is proposed. Six E-nose instruments, including one master instrument and five slave instruments designed with the same types of sensors and other electrical components, were used to evaluate the performance of the proposed model. Simulated and experimental results for concentration estimation in real-time confirmed the efficiency of the proposed calibration transfer models and the enhanced intelligence of E-nose. The instrumental related signal shifts have been reduced significantly through the calibrated sensor responses and also proved our initial assumption of homogeneous linearity. In mass calibrations of instruments not limited in the E-nose system with metal oxygen semiconductor gas sensors, the proposed method can also be used in other systems according to the following three steps. First, a master instrument (standard instrument) should be determined. Second, a certain number of transfer samples (five in this paper) should also be needed in calibration through KSS algorithm when a new instrument (slave instrument) comes. Finally, the proposed method is directly used onto the obtained transfer samples measured on the master instrument and slave instrument to calculate the calibration coefficients. The calibration coefficients can be feasible in long term. This paper presents three chemical analytes to validate our method by an electronic nose with metal oxygen semiconductor sensors. The applicability of the proposed model still remains to be validated for real applications and measurements of other kinds of substances.

Acknowledgements

This work was supported by the Key Science and Technology Research Program (CSTC2010AB2002), Central University Postgraduate' Science and Innovation Funds of China (CDJXS10161114, 200911B1A0100326), Central University Postgraduate' Innovation Team Building Project (200909C1016).

References

[1] M.P. Marti, R. Boque, O. Busto, J. Guasch, Electronic noses in the quality control of alcoholic beverages, Trends Anal. Chem. 24 (2005) 57–66.
[2] J.S. Vestergard, M. Martens, P. Turkki, Application of an electronic nose system for prediction of sensory quality changes of a meat product (pizza topping) during storage, LWT 40 (2007) 1095–1101.
[3] H. Yu, J. Wang, Discrimination of Long Jing Green-tea grade by electronic nose, Sens. Actuators B: Chem. 122 (2007) 134–140.
[4] R.M. Negri, S. Reich, Identification of pollutant gases and its concentrations with a multi-sensor array, Sens. Actuators B: Chem. 75 (2001) 172–178.
[5] A.P.F. Turner, N. Magan, Electronic noses and disease diagnostics, Nat. Rev. Microbiol. 2 (2004) 161–166.
[6] M. Bicego, G. Tessari, G. Tecchilli, M. Bettinelli, A comparative analysis of basic pattern recognition techniques for the development of small size electronic nose, Sens. Actuators B 85 (2002) 137–144.
[7] P. Ciosek, W. Wroblewski, The analysis of sensor array data with various pattern recognition techniques, Sens. Actuators B 114 (2006) 85–93.
[8] K. Ihokura, J. Watson, The Stannic Oxide Gas Sensor, CRC, Boca Raton, FL, 1994.
[9] E.J. Wolfrum, R.M. Meglen, D. Peterson, J. Sluiter, Calibration transfer among sensor arrays designed for monitoring volatile organic compounds in indoor air quality, IEEE Sens. J. 6 (2006) 1638–1643.
[10] E. Bouveresse, D.L. Massart, Standardisation of near-infrared spectrometric instruments: a review, Vib. Spectrosc. 11 (1996) 3–15.
[11] E. Bouveresse, C. Hartmann, D.L. Massart, Standardization of near-infrared spectrometric instruments, Anal. Chem. 68 (6) (1996) 982–990.
[12] J. Sjoblom, O. Svensson, M. Josefson, H. Kullberg, S. Wold, An evaluation of orthogonal signal correction applied to calibration transfer of near infrared spectra, Chemom. Intell. Lab. Syst. 44 (1998) 229–244.
[13] B. Walczak, E. Bouveresse, D.L. Massart, Standardization of near-infrared spectra in the wavelet domain, Chemom. Intell. Lab. Syst. 36 (1997) 41–51.
[14] K.S. Park, Y.H. Ko, H. Lee, C.H. Jun, H. Chung, M.S. Ku, Near-infrared spectral data transfer using independent standardization samples: a case study on the trans-alkylation process, Chemom. Intell. Lab. Syst. 55 (2001) 53–65.
[15] C. Dinatale, F.A. Davide, A. Damico, W. Gopel, U. Weimar, Sensor array calibration with enhanced neural networks, Sens. Actuators B: Chem. 18 (1994) 654–657.
[16] S. Osowski, et al., Neural methods of calibration of sensors for gas measurements and aroma identification system, J. Sens. Stud. 23 (4) (2008) 533–557.
[17] P. Laurent, O.B. Jacques, T. Raphael, Data transferability between two MS-based electronic noses using processed cheeses and evaporated milk as reference materials, Eur. Food Res. Technol. 214 (2002) 160–162.
[18] F.C. Tian, S.X. Yang, K. Dong, Circuit and noise analysis of odorant gas sensors in an E-nose, Sensors 5 (2005) 85–96.
[19] X.T. Xu, F.C. Tian, S.X. Yang, Q. Li, J. Yan, J.W. Ma, A solid trap and thermal desorption system with application to a medical electronic nose, Sensors 8 (2008) 6885–6898.
[20] F.C. Tian, X.T. Xu, Y. Shen, J. Yan, Q.H. He, J.W. Ma, T. Liu, Detection of wound pathogen by an intelligent electronic nose, Sens. Mater. 21 (2009) 155–166.
[21] L.H. Zhang, W.L. Xu, C. Chang, Genetic algorithm for affine point pattern matching, Pattern Recogn. Lett. 24 (2003) 9–19.
[22] J. Heikkilä, Pattern matching with affine moment descriptors, Pattern Recogn. 37 (2004) 1825–1834.
[23] S. Haykin, Neural Networks, a Comprehensive Foundation, Macmillan, New York, NY, 2002.
[24] D. Gao, M. Chen, J. Yan, Simultaneous estimation of classes and concentrations of odors by an electronic nose using combinative and modular multilayer perceptrons, Sens. Actuators B 107 (2005) 773–781.
[25] B. Yea, T. Osaki, K. Sugahara, R. Konishi, The concentration estimation of inflammable gases with a semiconductor gas sensor utilizing neural networks and fuzzy inference, Sens. Actuators B 41 (1997) 121–129.
[26] Gas concentration estimation in ternary mixtures with room temperature operating sensor array using tapped delay, architectures, Sens. Actuators B 124 (2007) 309–316.
[27] M. Pardo, G. Sberveglieri, Remarks on the use of multilayer perceptrons for the analysis of chemical sensor array data, Sens. J. IEEE 4 (3) (2004) 355–363.
[28] D.L.A. Fernandes, M. Teresa, S.R. Gomes, Development of an electronic nose to identify and quantify volatile hazardous compounds, Talanta 77 (2008) 77–83.
[29] Štěpán Obdržálek, Jiří Matas, Object recognition using local affine frames on distinguished regions, BMVC (2002) 113–122.
[30] R.M. Heiberger, R.A. Becker, Design of an S function for robust regression using iteratively reweighted least squares, J. Comput. Graph. Stat. 1 (1992) 181–196.

[31] F. Sales, M.P. Callao, F.X. Rius, Multivariate standardization for correcting the ionic strength variation on potentiometric sensor arrays, Analyst 125 (2000) 883–888.
[32] Y.H. Huang, D. Jiang, D.F. Zhuang, J.Y. Fu, Evaluation of hyperspectral indices for chlorophyll-a concentration estimation in Tangxun Lake (Wuhan, China), Int. J. Environ. Res. Public Health 7 (2010) 2437–2451.

Biographies

Lei Zhang received his bachelor degree in electrical/electronics engineering in 2009 from the Nanyang Institute of Technology, China; from September 2009 to December 2010, he studied for a MS degree in signal and information processing. He is presently with Chongqing University, pursuing his Ph.D. degree in circuits and systems. His research interests include computational intelligence, artificial olfactory system, and nonlinear signal processing in electronic nose.

Fengchun Tian received Ph.D. degree in 1997 in electrical engineering from Chongqing University. He is currently a professor with the College of Communication Engineering of Chongqing University. His research interests include electronic nose technology, artificial olfactory systems, pattern recognition, chemical sensors, signal/image processing, wavelet, and computational intelligence. In 2006 and 2007, he was recognized as a part-time professor of GUELPH University, Canada.

Chaibou Kadri received his bachelor degree in electrical/electronics engineering in 2001 from the Federal University of Technology Bauchi, Nigeria; his MS degree in communication and information system in 2009, from Chongqing University, China. He is presently with Chongqing University, pursuing his Ph.D. degree in circuits and systems. His research interests include signal processing for gas sensors array instruments, and machine learning.

Bo Xiao received his bachelor degree in college of communication engineering in 2010 from the Chongqing University, China; from September 2010 to December 2011, he studied for a MS degree in signal and information processing. His research interests include artificial olfactory system and electronic nose technology.

Hongjuan Li received her bachelor degree in college of communication engineering in 2009 from the Chongqing University, China; from September 2009 to December 2011, she studied for a MS degree in circuits and system. Her research interests include circuits and system design in electronic nose technology.

Lina Pan received her bachelor degree in college of communication engineering in 2009 from the Chongqing University, China; from September 2009 to December 2011, she studied for a MS degree in signal and information processing. Her research interests include artificial olfactory system and electronic nose technology.

Hongwei Zhou received his bachelor degree in Faculty of Physics and Opto-Electronic Engineering, Taiyuan University of Technology; from September 2008 to December 2011, he studied for a MS degree in signal and information processing in college of communication engineering, Chongqing University, China; his research interests include circuits and system design, signal processing technology in electronic nose application.